Molecular insights into Electronic and Optical Properties of Novel Diaminonaphthalene Derivatives for Dye Sensitized-Solar Cells

F. E. Abeng[1*], U. U. Udoka[2], N. N. Oji[3], D. O. Ofem[3] and F. L. Abeng[4]

[1]*Materials and Electrochemistry Research Group, Department of Chemistry, University of Cross River State, Calabar, Nigeria*
[2]*Theoretical Unit, Department of Pure and Applied Chemistry, University of Calabar, Cross River State*
[3]*Science Laboratory Technology), Federal Polytechnic Ugep, University of Cross River State*
[4]*Department of Physics, University of Cross River State, Calabar, Nigeria*
Corresponding author: fidelisabeng@unicross.edu.ng

Received 30/07/2025; accepted 05/01/2026
https://doi.org/10.4152/pea.2027450514

Abstract
Density functional theory (DFT) has been used to calculate electrical and photovoltaic properties of diaminonaphthalene and its derivatives, and optimize them. Findings demonstrated that time-dependent DFT investigations employing Coulomb-attenuated hybrid method with polarized split-valence 6-311G (d,p) basis sets and polarizable continuum model were able to predict excitation energies and spectra of the compounds in a reasonable manner. Levels of Energy of Highest Occupied and Lowest Unoccupied Molecular Orbitals from these compounds can have a positive effect on electron injection and dye renewal processes. Energy gap, short-circuit current density, light-harvesting efficiency, thermodynamic injection driving force and open-circuit photovoltage allowed for qualitative predictions about the reactivity of the different dyes.

Keywords: density functional theory; diaminonaphthalene; dye-sensitized solar cells; electronic and optical properties.

Introduction•

Organic dyes and several metal complexes have been produced and used as sensitizers. A lot of interest has been paid to dye-sensitized solar cells (DSSC) as inexpensive alternatives to traditional solid-state photovoltaic systems [1-3]. The effectiveness of each technique used in DSSC has been the focus of numerous studies [4]. The dye serves as a sensitizer in DSSC by absorbing solar energy, which is then converted to electrical energy [5]. Large light absorption coefficients and simple redox potential control, which are connected to the positions of highest occupied and lowest unoccupied molecular orbitals (HOMO and LUMO,

•The abbreviations and symbols definition lists are in pages 570-71.

respectively), are two benefits of organic dyes. The maximum efficiency of DSSC with metal complexes adsorbed on nanocrystalline titanium dioxide (TiO_2) is 13%, so far [6]. Other benefits of DSSC that have yet to be realized include colour, transparency and advances in power density. There is a critical need to develop environmentally acceptable sources of energy that can meet the world's rising energy demands in a time when environmental threats are alarmingly real. The five components that typically make up a DSSC include: the molecular dye that absorbs light; a wide band gap semi-conductor (TiO_2); a redox electrolyte – typically, iodide/triiodide redox couple (I^-/I_3^-); a counter electrode (normally, a piece of glass coated with platinum); and a porous layer that serves as the anode made of TiO_2 nanoparticles [7]. As a result of electron injection, which happens when sunlight sensitizes molecular dyes, excited electrons flow into the semiconductor's conduction band. In order to complete the circuit and power the load, electrons from TiO_2 flow to the transparent electrode. They flow back to the electrolyte through the counter electrode after passing through the external circuit. The electrons are subsequently sent back to the molecular dye by the electrolyte, which also regenerates the oxidized dye [8]. It is important to remember that each dye conducts, at different degrees of absorption [8].

To determine whether the unique four dyes of the present study are suitable for such an application, it was investigated how conductive they are in relation to solar cells. The selection of these azo dyes was based on their strong reactive properties and high absorption to light, which were studied using density functional theory (DFT) and time-dependent-DFT analyses of photovoltaic performance. These analyses included: short-circuit current density (J_{sc}), light harvesting efficiency (LHE), charge injection efficiency, thermodynamic injection driving force (ΔG_{inject}), oxidation potential of the dye at excited and ground states, dye regeneration energy, open-circuit voltage (V_{OC}), and reorganization energy parameters, along with detailed frontier molecular orbital (FMO), natural bond orbital (NBO), global reactivity descriptors and density of state parameters, absorption and solvatochromism to investigate HOMO-LUMO energies, second order perturbation energies, structure reactivity, contributions of molecular orbitals, response to light of the different structures in different media and vibrational energy distribution analysis (VEDA).

Methodological and computational details

Electronic Structure Theory based on DFT and B3LYP with 6-31+G(d,p) basis set was used to describe and optimize ground state geometrical structures of azo compounds. The structures were given the co-names dyes A, B, C and D, respectively. Theoretical analysis of organic dyes for DSSC applications extensively employed DFT computational method. In order to confirm that

optimized geometries were genuine energy minima, frequency calculations were also performed using the same level of theory [9]. None of the frequency calculations produced untrue frequencies. First five singlet states' vertical excitation energies were calculated using long-range CAM-B3LYP/6-31+G(d,p) DFT technique in gas, ethanol, acetone and water media. Electronic excitation energies were calculated using CAM-B3LYP functional since it offers the best overall performance, and no correlation between excitation energy errors and accurate values was observed [20]. With the aid of Gaussian09W and GaussView 6.0.16 software suite, all computational calculations were carried out using DFT. Multiwfn 3.7 (dev) function analyzer32, which is free to download from http://sobereva.com/multiwfn, was used for surface and structural analysis. Gaussian 3.1 method built inside Gaussian 09 software was employed to compute NBO. VEDA 4 program assigned all vibrational wave numbers of the different investigated substances based on potential energy distribution.

By using well-known Koopman's theorem, molecular electronic characteristics and reactivity of the dyes were estimated at DFT/6-31+(d,p) level of theory. E_{HOMO} and E_{LUMO} (energies of HOMO and LUMO) indicate whether a dye is ready to be attacked by electrophiles or nucleophiles, respectively. So that DSSC in which TiO_2 is employed as conduction band is effective, the researched dyes had to have a specific set of characteristics. E_{LUMO} of the dye had to be higher than conduction band edge (ECB) of TiO_2 (-4.0 eV) [10]. This is significant because DSSC performance can be enhanced by quick electron injection from the excited states of the dyes to TiO_2 conduction band. To allow for charge regeneration of the dyes, E_{HOMO} of the dye had to be below redox potential of I^-/I_3^- couple (-4.80 eV). ΔE_{LUMO} is defined as the difference between energy gaps (E_{gap}) of the dyes' E_{LUMO} and TiO_2's E_{CB}. It can be expressed numerically as:

$$\Delta E_L = E_{LUMO} - E_{CB}\ (TiO_2) \quad (1)$$

ΔE_{HOMO} is described as the difference of E_{redox} of I^-/I^-_3 and E_{HOMO} of the dyes. It is mathematically represented as:

$$\Delta E_H = E_{redox}\ (I^-/I^-_3) - E_{HOMO} \quad (2)$$

ΔE_H is E_{gap} between E_{HOMO} and E_{LUMO} of the dyes. It is mathematically represented as:

$$\Delta E_H = E_{LUMO} - E_{HOMO} \quad (3)$$

E_{LUMO} is used to estimate electron affinity (EA) and E_{HOMO} is related to ionization potential (IP), according to molecular orbital theory approaches [11-12]. This makes it possible to calculate other quantum chemical descriptors like hardness, softness, electronegativity and electrophilicity index. IP and EA for DSSC explain

energy barrier for both electrons and holes. Mathematical representation of IP and EA is:

$$IP = -E_{HOMO} \quad (4)$$

$$EA = -E_{LUMO} \quad (5)$$

For both holes and electrons to be able to donate and accept holes, it is crucial to know IP and EA values. Increased hole-creating capacity requires a low IP. Increasing electron-accepting ability requires a greater EA [13]. Electronegativity (c), chemical potential (m), hardness (h), electrophilicity index (u), electro-accepting (h), electro-accepting power (u+), and electro-donating (u-) can all be redefined for closed shell molecules using Koopman's theorem as follows:

$$x = \frac{IP+E}{2} \quad (6)$$

$$\mu = \frac{E_{HOMO}+ E_{LUMO}}{2} \quad (7)$$

$$\eta = \frac{IP-E}{2} \quad (8)$$

$$w = \frac{\mu^2}{2\eta} \quad (9)$$

Results and discussion

Frontier molecular Orbitals (FMO)

Based on experimental conditions, reactive dyes were optimized and computed using four essential solvents. Derived values for HOMO, LUMO, E_{gap} and global reactivity descriptors of the dyes were carefully analysed, as reported in Table 1.

Table 1: Quantum chemical descriptors for dyes A, B, C and D in gas phase.

Quantum chemical descriptors	Dye A	Dye B	Dye C	Dye D
E_{Homo}	-5.59874	-5.79874	-5.64963	-5.20717
E_{Lumo}	-3.23407	-3.42047	-3.33013	-2.87189
Eg	2.364	2.37827	2.3195	2.33528
x	-4.41640	-4.60960	-4.44185	-4.03953
-μ	4.41640	4.60960	4.44185	4.03953
ɳ	1.18232	1.18913	1.15975	1.16764
W	8.24836	8.93443	8.50615	6.98751
δ	2.36467	2.37827	2.3195	2.33528

The analysis presented in Table 1 indicated that E_{LUMO} values of all studied particles are much higher than TiO_2's conduction band (-4.7 eV). Therefore, the studied particles have strong ability to inject electrons into TiO_2 electrodes. The test phenomenon is in perfect accord with earlier published work [15-19]. Additionally, because E_{HOMO} levels are lower than I^-/I_3^- electrolyte's reduction potential energy (-

4.80 eV), it is possible for the oxidized dyes to be effectively regenerated from the reduced species in the electrolyte, resulting in an effective charge separation [8, 20]. All interactional corrections between electrons in the molecule's structure were made using DFT computations. Geometrical optimization of the structure was therefore determined using DFT technique, which is thought to be accurate and dependable. The study structures' geometry optimization findings are in Fig. 1 (A-D), which displays energy levels in the dyes from HOMO to LUMO.

The relative arrangement of occupied orbital and hypothetical orbit provides a reasonable qualitative indication of excitation properties [14], making the contribution of FMO very important in determining states of charge separation of investigated particles.

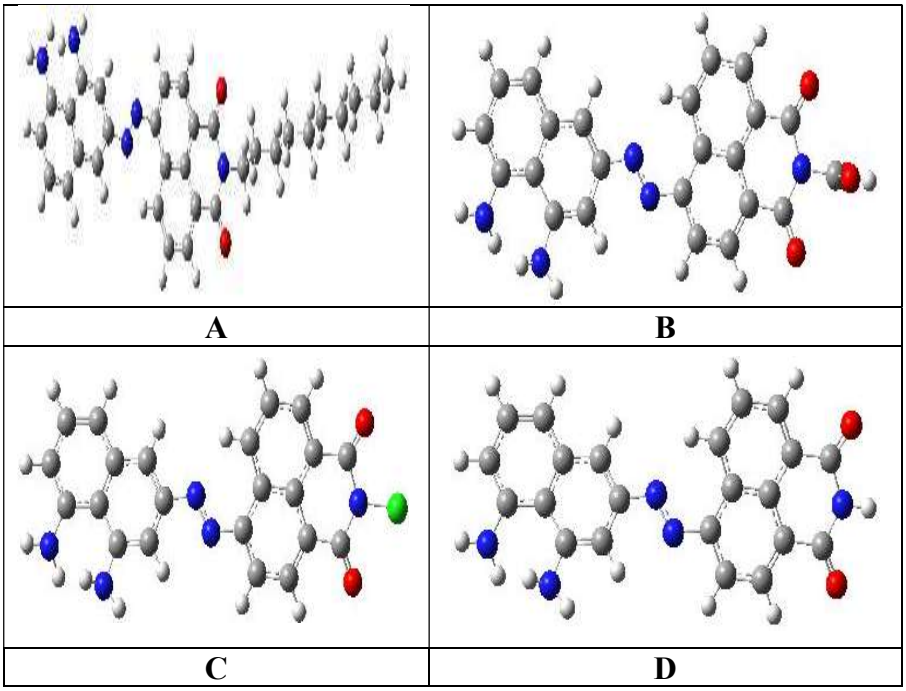

Figure 1: FMO structures of dyes A, B, C and D.

Distorted structures had an impact on the distribution of electron density and energy levels at HOMO, LUMO and E_{gap}. Presentation of subgroups causes a dramatic change in LUMO energy. This indicates that both effect of structural variations and kind of substitution play important roles in electronic properties. It is possible to see how HOMO and LUMO energy differ.

The following is a classification of band gap calculated from Diaminonaphthalene and its derivatives: B>A>C>D. Absorption wavelength was converted from E_{gap}, an important parameter.

According to the coordination of each dye in the ground state, Fig. 2 depicts 3D distribution of HOMO and LUMO of the compounds examined, due to linear combination of atomic orbital molecular orbitals [21].

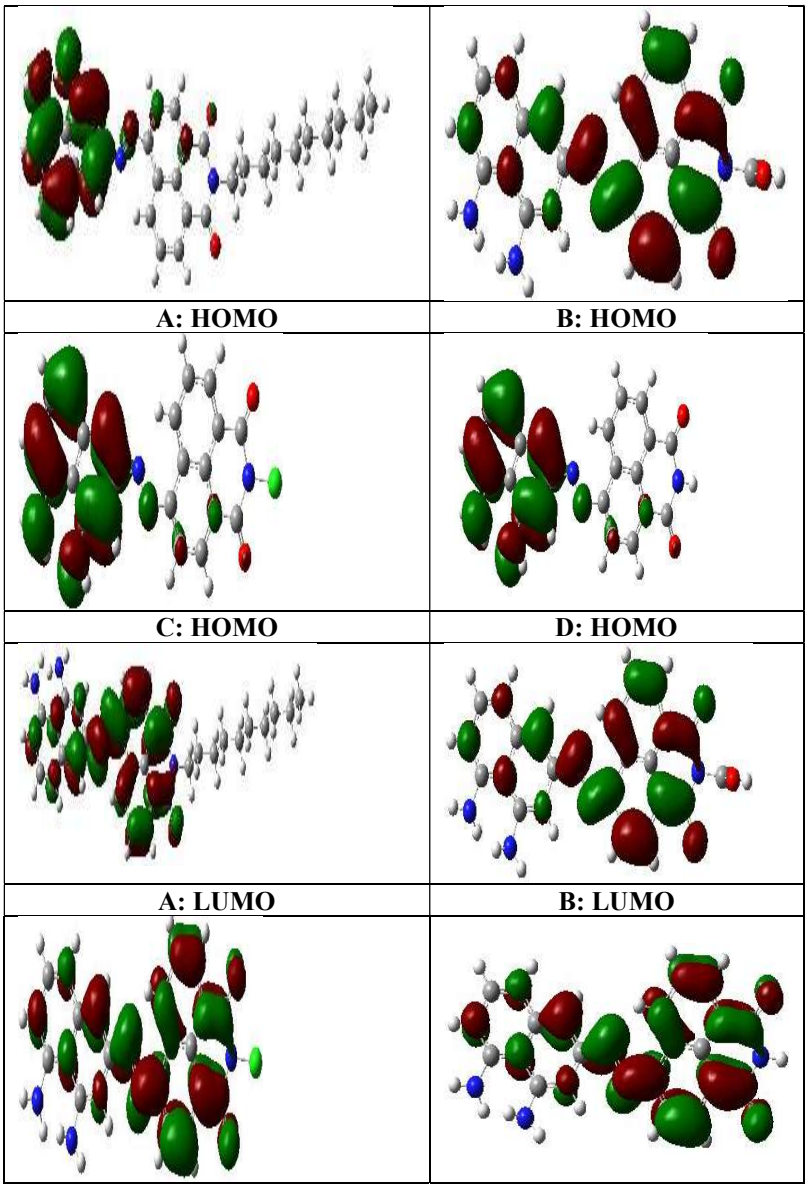

Figure 2: HOMO and LUMO frontier orbital distribution of dyes obtained at B3LYP/6-31+G(d,p) basis set.

Generally, LUMO has an antibonding and link-character in the centre of the subunits, while HOMO molecules have a π −bonding and antibonding mechanism between succeeding subunits.

Photovoltaic properties

Energy difference between quasi-Fermi level of the semiconductor's conduction band (TiO_2) and redox potential of electrolyte's redox couple I^-/I_3^- is known as V_{OC}. It is denoted mathematically as:

$$V_{oc} = \frac{E_{cB}+\Delta CB}{q} + \frac{kT}{q}\, in\, \left(\frac{n_c}{NcB}\right) - \frac{E_{Redox}}{q} \qquad (10)$$

where n_c is the number of electrons in the conduction band, N_{cB} is density of accessible states in conduction band, E_{Redox} is redox potential of the electrolyte,

E_{CB} is TiO_2 conduction band edge, q is unit charge, k is Boltzmann constant and T is absolute temperature [22]. When the dyes are absorbed, N_{CB} shifts from CB. It is denoted mathematically as:

$$\Delta_{CB} = \frac{q\mu_{normal}\gamma}{\varepsilon_o \varepsilon} \quad (11)$$

where q is the dye concentration on the surface, μnormal is dipole moment of each dye molecule perpendicular to the surface of TiO_2, and ε_o and ε are vacuum and dielectric permittivities, respectively. The difference between E_{LUMO} and E_{CB} can also be used to calculate V_{OC} [23].

$$V_{oc} = E_{LUMO} - E_{CB} \quad (12)$$

Because the examined dyes are not individually adsorbed on TiO_2, it is employed for this purpose. As a result, J_{sc} calculations can be done using the equation:

$$J_{SC} = \int LHE\ (\lambda)\phi_{Injection}\eta_{collect}d\lambda \quad (13)$$

where $\phi_{Injection}$ is electron injection efficiency, $\eta_{collect}$ is charge collecting efficiency and LHE (λ) is LHE at maximum wavelength. LHE and $\phi_{Injection}$ should be as high as possible to achieve a high J_{sc}. Mathematical formulation for LHE is:

$$LHE = 1 - 10^{-f} \quad (14)$$

where $\phi_{Injection}$ is connected to ΔG_{inject} from excited states of dye to conductive band TiO_2 and f is oscillator strength of the dye corresponding to λ max. Mathematical formula for ΔG_{inject} (free energy difference for ΔG_{inject}) is:

$$\Delta G_{inject} = E^{dye*} - E_{CB}^{TIO_2} \cong E^{dye} + \Delta E - E_{CB}^{TIO_2} \quad (15)$$

where E^{dye*} and E^{dye} are excited and ground states' redox potential for the oxidized dye, respectively, ΔE is lowest vertical excitation energy and $E_{CB}^{TIO_2}$ is the energy of conductive band edge of TiO_2.

$$\Delta G_{reg.} = \mu(I^-/I_3^-) - E^{dye} \quad (16)$$

where ΔG_{reg} is driving force for dye regeneration [24].

Effective electron injection for an oxidized dye may have ΔG_{inject} value higher than 0.2 eV. Computed values of LHE, ΔG_{inject}, ΔG_{reg}, V_{OC}, ΔG_{cr} and J_{sc} in gas phase are given in Table 2.

It is crucial to remember that, while calculating ΔG_{reg}, TiO_2 semiconductor's experimentally determined ECB value was 4.00 Ev [25-28]. When ΔG_{inject} values were higher than 0.2 Ev, all four dyes in the gas phase effectively injected electrons. Values of ΔG_{inject} for dye A, C and D were higher, thus providing more electron injection. Additionally, it is noted that ΔG_{reg} values for each of the four dyes were lower than 0.4 eV. This indicates that the dyes had little to no impact on

ΔG_{reg}. According to Table 2 findings, LHE values varied and were more stable in dyes A, C and D, which maintained highest V_{OC} values.

Table 2: Photovoltaic properties of the four dye molecules in gas phase.

Ev	Dye A	Dye B	Dye C	Dye D
LHE	0.8897	0.2530	0.6089	0.4896
ΔG_{inj}	1.1452	0.5705	1.1383	1.1281
ΔG_{reg}	-1.7929	-1.3795	-1.7029	-1.9281
V_{oc}	2.6258	0.5795	2.5673	2.5628
ΔG_{cr}	-4.6871	-3.8295	-3.6871	-4.3781
J_{sc}	2.4629	2.6226	2.5629	2.4313

Natural bond orbital analysis

In order to chemically understand the nature and type of interaction that exists between Lewis and non-Lewis orbitals of the dye molecules under study, the study of NBO analysis was conducted. Charge exchange and conjugative contact between orbitals of donor and acceptor are recognized in this interaction. This approach takes into account variations in energy of interaction between donors and acceptor orbitals, which are reported as second order perturbation energies, and derived from second order perturbation theory of Fock matrix [29]. Eq. (17) was used to calculate stabilization energy (E2) or donor-acceptor NBO interaction energy (E) between the orbitals under discussion.

$$E^{(2)} = q_i \frac{(F_i,j)^2}{E_i - E_i} \quad (17)$$

where q_i is orbital occupancy $E_i - E_i$ is the diagonal elements and F_i, j is the off diagonal NBO fock matrix element.

In order to explain the inter- and intra-molecular hydrogen bonding and p electron delocalization inside the molecule, NBO analysis was calculated at the same level of theory as the optimized structures [30-33]. In the second order perturbation result shown in Table 3, several interactions have been noticed. as bonding, nonbonding, and anti-bonding interactions with varying energies depending on the degree of the connection. The most noticeable and greatest interactions occur between lone pairs on carbon and hetero atoms, which are characterized as non-bonding interactions and have been shown to improve molecular stability.

In Dye A, second order perturbation energies of donor-acceptor interactions in $\pi^*(C_{28}$ - $C_{30}) \rightarrow \delta^*(N_{38}$-$H_{40})$, $\pi^*(C_{28}$-$C_{30}) \rightarrow \delta^*(C_{10}$-$C_{16})$, $\pi^*(C_{31}$-$C_{33}) \rightarrow \delta^*(C_{26}$-$C_{30})$, had E^2 values of 11,863.48, 3,945.63 and 1,352.24 kJ/mol^{-1}, respectively, which confers stronger stability to the structure. For Dye B $\pi^*(C_{28}$-$C_{31}) \rightarrow \pi^*(C_4$ - $C_5)$ had $E^{(2)}$ value of 12,128.86 kJ/mol^{-1} and $LP_{(3)}\ O_{46} \rightarrow \pi^*(C_{44}$-$C_{45})$ had $E^{(2)}$ value of 3,305.14 kj/mol^{-1}. These strong stabilization energies seen in the molecule give high stability to the dye molecule.

Electron donation from $LP_{(1)}\ O_{46} \rightarrow \pi^*(C_{28}$ - $C_{31})$, $LP_{(3)}\ O_{46} \rightarrow \pi^*(C_{28}$ - $C_{31})$ and $LP_{(3)}\ O_{46} \rightarrow \pi^*(C_{34} – C_{35})$ shows $E^{(2)}$ values of 2,588.27, 2,326.17 and 1,995.68 kJ/mol^{-1}, respectively. These are high stabilization energies that will also confer a greater stability on the molecule. Dye C has the highest second order.

Perturbation energies $E^{(2)}$ of 819.20 kJ/mol^{-1} are seen in LP (1) $Cl_{44} \rightarrow \delta^*$ (N_{41}-H_{42}) and of 311.18 kJ/mol^{-1} for π^*(C_{28}-C_{30}) $\rightarrow$ π^*(C_{23} - C_{25}). In Dye D, second order perturbation energies of donor-acceptor interactions in π^*(C_{59}-C_{61}) $\rightarrow$ BD*(C_{54}-C_{56}), π^*(C_{59}-C_{61}) $\rightarrow$ π^*(C_{55}-C_{57}), π^*(C_3-C_4) $\rightarrow$ π^*(C_{10}-C_{12}), π^*(C_{63}-C_{65}) $\rightarrow$ π^*(C_{62}-C_{64}) and π^*(C_3-C_4) $\rightarrow$ π^*(C_9 -C_{13}) had $E^{(2)}$ values of 298.88, 268.95, 252.78, 221.51 and 214.25 kj/mol^{-1}, respectively, which confers stronger stabilization to the structure.

Absorption properties

A novel material's ability to absorb light according to the solar spectrum is crucial for its use as a photoelectric material. A good PV material should have excellent visual absorption capabilities that are both broad and uniform [34-35]. Utilizing time-dependent-DFT/B3LYB, molecules' excitation state was investigated. Values of absorption energy (eV), absorption wavelength (λ max in nm), oscillators' strength, main assignment (HOMO-LUMO) and transition characteristics (%) are shown in Table 3.

Table 3: Most significant interactions of second order perturbation energies of the dyes.

Dye	Donor NBO (i)	Acceptor NBO (j)	$E^{(2)}$ Kcal/mol	$E_{(j)}$- $E_{(i)}$ a.u	$F_{(i,j)}$
	$\pi^* C_{28} - C_{30}$	$\sigma^* N_{38} - H_{40}$	11,863.48	0.07	1.624
	$\pi^* C_{28} - C_{30}$	$\sigma^* C_{10} - C_{16}$	3,945.63	0.14	1.273
	$\pi^* C_{31} - C_{33}$	$\sigma^* C_{26} - C_{30}$	1,352.24	0.50	1.865
	$\pi^* C_{31}$ - C_{33}	$\sigma^* N_{41} - H_{43}$	1,220.90	0.14	0.965
Dye	$\pi^* C_{31} - C_{33}$	$\pi^* C_{28} - H_{30}$	1,150.38	0.77	1.348
A	$\pi^* C_{28}$ - C_{30}	$\sigma^* C_{13} - H_{33}$	932.10	0.49	1.201
	$\pi^* C_{31} - C_{33}$	$\sigma^* C_{10} - C_{16}$	829.07	0.91	1.851
	$\pi^* C_{31} - C_{33}$	$\sigma^* N_{38} - H_{40}$	819.70	0.84	1.932
	$\pi^* C_{28} - C_{30}$	$\pi^* C_{10} - C_{12}$	753.52	0.58	0.941
	$\pi^* C_{28} - C_{30}$	$\sigma^* N_{38} - H_{39}$	428.16	1.06	1.199
	$\pi^* C_{28} - C_{31}$	$\sigma^* C_4 - C_5$	12,128.86	0.22	2.961
	$LP3$ 046	$\sigma^* C_{44} - C_{45}$	3,305.14	0.32	0.984
	$LP1$ 046	$\sigma^* C_{28} - C_{31}$	2,588.27	0.20	0.644
	$LP3$ 046	$\sigma^* C_{28} - H_{31}$	2,326.17	0.42	1.006
Dye	$LP1$ 046	$\pi^* C_{34} - H_{35}$	1,995.68	0.46	0.972
B	$\pi^* C_{44}$ - C_{45}	$\sigma^* C_{34} - H_{55}$	1,849.89	0.24	0.592
	$\pi^* C_{28} - C_{31}$	$\sigma^* C_{25} - C_{31}$	1,746.58	0.10	1.115
	$\pi^* C_{31} - C_{33}$	$\sigma^* C_{44} - H_{46}$	1,576.06	1.11	2.225
	$\pi^* C_{44} - C_{45}$	$\pi^* C_{34} - H_{35}$	1,135.48	0.14	1.061
	$\sigma^* C_{44} - C_{46}$	$\sigma^* C_{44} - O_{45}$	877.06	0.53	1.549
	$LP_{(1)}$ CL_{44}	$\sigma^* N_{41} - H_{42}$	819.20	1.01	0.813
	$\pi^* C_{28} - C_{30}$	$\pi^* C_{23} - C_{25}$	311.18	0.01	0.080
	$\pi^* C_{28} - C_{30}$	$\pi^* C_{24} - C_{26}$	282.05	0.01	0.075
	$\pi^* C_{32} - C_{34}$	$\pi^* C_{31} - C_{33}$	211.84	0.01	0.078
Dye	$\pi^* C_3 - C_4$	$\pi^* C_9 - C_{13}$	201.33	0.01	0.078
C	$\sigma N18 - Cl_{44}$	$\sigma^* N_{41} - H_{42}$	196.48	0.82	0.360
	$LP1$ Cl_{44}	$\sigma^* N_{41} - H_{43}$	155.72	1.82	0.477
	$LP_{(1)}$ Cl_{44}	$\sigma^* C_{25} - H_{29}$	140.79	1.27	0.378
	$\pi^* C_{17} O_{20}$	$\sigma^* C_5 - C_6$	104.31	0.02	0.075
	$LP_{(1)}$ N_{18}	$\pi^* C_{17} - O_{20}$	46.35	0.29	0.106
	$BD^*_{(2)} C_{59} - C_{61}$	$BD^*_{(2)} C_{59} - C_{61}$	298.88	0.01	0.081
	$\pi^* C_{59} - C_{61}$	$\pi^* C_{55} - C_{57}$	268.95	0.01	0.076
	$\pi^* C_3 - C_4$	$\pi^* C_{10} - C_{12}$	252.78	0.01	0.079
	$\pi^* C_{63} - C_{65}$	$\pi^* C_{62} - C_{64}$	221.51	0.01	0.078
Dye	$\pi^* C_3 - C_4$	$\pi^* C_9 - C_{13}$	214.25	0.01	0.079
D	$\pi^* C_{59} - C_{61}$	$\pi^* C_{62} - C_{64}$	209.53	0.01	0.079
	$\pi^* C_{17} - C_{20}$	$\pi^* C_5 - C_6$	101.55	0.02	0.076
	$\pi^* C_{16} - O_{19}$	$\pi^* C_{10} - C_{12}$	93.25	0.02	0.075
	LP1 N18	$\pi^* C_{17} - O_{20}$	55.77	0.26	0.111
	LP1 N18	$\pi^* C_{16} - O_{19}$	54.71	0.27	0.111

It can be stated that the dyes under research had computed maximum wavelengths from 492.08 to 705.85 nm. Additionally, findings showed that lowest singlet electronic excitation is described as a typical $n \rightarrow \pi^*$ transition, where low energy is necessary. Generally speaking, a dye's ability to absorb light depends greatly on the type of extra component [36]. Order of E_{gap} and wavelength for the dyes are consistent, meaning that the more redshift in UV-vis absorption, the shorter the E_{gap}, which suggests that the more polar the solvent, the narrower the band gap [36].

Conclusions

HOMO and LUMO calculations of the investigated dyes showed that, when alternative structures were taken into account, their E_{gap} values were comparable to those of semiconductor materials, where molecular modifications had an impact on electronic properties. E_{HOMO} and E_{LUMO} levels of the dyes are well in line with requirements for an effective photosensitizer. E_{LUMO} levels of all dyes are higher than conduction band of dyes or TiO_2. An electron from the dyes can be injected into the conduction band of dyes or TiO_2, followed by regeneration in a sensitive organic solar cell. On the other hand, the dyes demonstrated improved electron injection efficiency with $\Delta G_{injection}$ positive values and negative values of ΔG_{reg}, which are favourable for dyes. Based on efficiency results, it can be said that the researched dyes' appearance absorption energy and wavelength requirements match those of the solar spectrum. Considering the study's findings, all of the compounds under consideration can be utilized as sensitizers.

Authors' contributions

F. E. Abeng: conceptualization; methodology; supervision; writing original draft. **U. U. Udoka**: methodology; project administration; reviewing and editing. **N. N. Oji**: funding acquisition; data curation. **D. O. Ofem**: validation, formal analysis. **F. L. Abeng**: software formal analysis.

Abbreviations

CAM-B3LYP: Coulomb-attenuated hybrid functional
DFT: Density Functional Theory
DSSC: dye-sensitized solar cells
EA: electron affinity
ECB: Energy conduction band edge
E_{gap}: energy gap
E_{HOMO}: Energy of Highest Occupied Molecular Orbital
E_{LUMO}: Energy of Lowest Occupied Molecular Orbital
FMO: Frontier molecular orbital
HOMO: Highest Occupied Molecular Orbital
I^-/I_3^-: iodide/triiodide redox couple
IP: ionization potential
J_{sc}: short-circuit current density
k: Boltzmann constant
LHE: Light Harvesting Efficiency
LUMO: Lowest Occupied Molecular Orbital

NBO: Natural Bond Orbital
q: unit charge
T: absolute temperature
TiO_2: titanium dioxide
VEDA: vibrational energy distribution analysis
V_{OC}: open-circuit voltage

Symbols definition

$\Delta G_{injection}$: thermodynamic injection driving force
ΔG_{reg}: thermodynamic driving force for dye regeneration
E_{Redox}: redox potential of the electrolyte
ε: vacuum permittivities
ε: dielectric permittivities
$\eta_{collect}$: charge collecting efficiency
n_c: number of electrons in the conduction band
λ: light harvesting efficiency at maximum wavelength
μ_{normal}: dipole moment of each dye molecule perpendicular to the surface of TiO_2,
$\phi_{injection}$: electron injection efficiency

References

1. Cabir B, Yildiko U, Ağirtaş M. Synthesis, DFT analysis, and electronic properties of new phthalocyanines bearing ETAEO substituents on peripheral position. J Coord Chem. 2019;72(17):2997-3011. https://doi.org/10.1080/00958972.2019.1680832
2. Agırtaş M, Güngördü D, Yildiko Ü et al. Design of novel substituted phthalocyanines; synthesis and fluorescence, DFT, photovoltaic properties. Turk J Chem. 2020;44(6):1574-86. https://doi.org/10.3906/kim-2007-40
3. Ghadari R, Saei P-S, Sabri A et al. Enhanced phthalocyanine-sensitized solar cell efficiency via cooperation of nitrogen-doped carbon dots. J Clean Prod. 2020;268:122236. https://doi.org/10.1016/j.jclepro.2020.122236
4. Mumit M, Pal T, Alam M et al. DFT studies on vibrational and electronic spectra, HOMO–LUMO, MEP, HOMA, NBO and molecular docking analysis of benzyl-3-N-(2,4,5-trimethoxyphenylmethylene)hydrazinecarbodithioate. J Mol Struct. 2020;1220(15):128715. https://doi.org/10.1016/j.molstruc.2020.128715
5. Ağırtaş M, Cabir B, Yıldıko Ü et al. Synthesis, antioxidant, DNA cleavage and antimicrobial properties of phthalocyanine complexes bearing the poly-hydroxyl groups. Chem Pap. 2021;75(4):1749-60. https://doi.org/10.1007/s11696- 020-01432-7
6. Devadiga D, Selvakumar M, Shetty P et al. Recent progress in dye sensitized solar cell materials and photo-supercapacitors: A review. J Pow Sour. 2021;493:229698. https://doi.org/10.1016/j.optmat.2020.110441
7. Mariotti N, Bonomo M, Fagiolari L et al. Recent advances in eco-friendly and cost-effective materials towards sustainable dye-sensitized solar cells. Green Chem. 2020;22:7168-218. https://doi.org/10.1039/D0GC01148G

8. Castillo-Robles J, Rocha-Rangel E, Ramírez-de-León J et al. Advances on Dye-Sensitized Solar Cells (DSSCs) Nanostructures and Natural Colorants: A Review. J Compos Sci. 2021;5:288. https://doi.org/10.3390/jcs5110288
9. Mejica GFC, Unpaprom Y, Balakrishnan D et al. Anthocyanin pigment-based dye-sensitized solar cells with improved pH-dependent photovoltaic properties. Sust Ener Tech Assess. 2022;51:101971. https://doi.org/10.1016/j.seta.2022.101971
10. Yuan Y, Wan C. Dual Application of Waste Grape Skin for Photosensitizers and Counter Electrodes of Dye-Sensitized Solar Cells. Nanomater. 2022;12:563. https://doi.org/10.3390/nano12030563
11. Jalali T, Arkian P, Golshan M et al. Performance evaluation of natural native dyes as photosensitizer in dye-sensitized solar cells. Opt Mater. 2020;110:110441. https://doi.org/10.1016/j.optmat.2020.110441
12. Kabir F, Manir S, Bhuiyan M et al. Instability of dye-sensitized solar cells using natural dyes and approaches to improving stability-An overview. Sustain Ener Techn Assess. 2022;52:102196. https://doi.org/10.1016/j.seta.2022.102196
13. Shi X, Li Y, Wang L. Two novel mono-hydroxyl pyranoanthocyanidins bearing dimethylamino substituent(s) for dye-sensitized solar cell. J Mol Struct. 2022;1252:132055. https://doi.org/10.1016/j.molstruc.2021.132055
14. Manzoor T, Niaz S, Pandith A. Exploring the effect of different coumarin donors on the optical and photovoltaic properties of azo-bridged push-pull systems: A theoretical approach. Int J Quant Chem. 2019;119:e25979. https://doi.org/10.1002/qua.25979
15. Mohankumar V, Pounraj P, Pandian M. Theoretical Investigation on Flavones and Isoflavones-Added Triphenylamine-Based Sensitizers for DSSC Application. Braz J Phys. 2019;49:103-12. https://doi.org/10.1007/s13538-018-00622-9
16. Sinopoli A, Calogero G, Bartolotta A. Computational aspects of anthocyanidins and anthocyanins: A review. Food Chem. 2019;297:124898. https://doi.org/10.1016/j.foodchem.2019.05.172
17. Madugula S, Yarasi S. Molecular design of porphyrin dyes for dye sensitized solar cells: A quantitative structure property relationship study. Int J Quant Chem. 2017;117:e25385. https://doi.org/10.1002/qua.25385
18. Hajizadeh F, Reisi-Vanani A, Azar Y. Theoretical design of Zn-dithiaporphyrins as sensitizer for dye-sensitized solar cells. Curr Appl Phys. 2018;18(10):1122-33. https://doi.org/10.1016/j.cap.2018.06.011
19. Terenti N, Giurgi G.-I, Szolga L et al. A. Effect of the Terminal Acceptor Unit on the Performance of Non-Fullerene Indacenodithiophene Acceptors in Organic Solar Cells. Mole. 2022;27:1229. https://doi.org/10.3390/molecules27041229
20. Hitler L, Izubundu B, Onyebuenyi A et al. Synthesis, characterization, and theoretical studies of the photovoltaic properties of novel reactive azonitrobenzaldehyde derivatives. RSC Adv. 2021;11;28433. https://doi.org/10.1039/D1RA05075C

21. Wu Y, Li C, Tian Z et al. Solar-driven integrated energy systems: State of the art and challenges. J Pow Sour. 2020;478:228762. https://doi.org/10.1016/j.jpowsour.2020.228762
22. Kokkonen M, Talebi P, Zhou J et al. Advanced research trends in dye-sensitized solar cells, J Mater Chem. 2021;9(17):10527-45. https://doi.org/10.1039/D1TA00690H
23. Ramya N, Nideep T, Nampoori V et al. The impact of ZnO nanoparticle size on the performance of photoanodes in DSSC and QDSSC: a comparative study. J Mater Sci Mater Electr. 2021;32(3):3167-79. https://doi.org/10.1007/s10854-020-05065-0
24. Choudhury B, Lin C, Shawon S et al. photoanode with hierarchical nanoforest TiO2 structure and silver plasmonic nanoparticles for flexible dye sensitized solar cell. Sci Rep. 2021;11(1):7552. https://doi.org/10.1038/s41598-021-87123-z
25. Akman E, Akin S, Ozturk T et al. Europium and terbium lanthanide ions co-doping in TiO2 photoanode to synchronously improve light harvesting and open-circuit voltage for high-efficiency dye-sensitized solar cells. Sol Ener. 2020;202(2):227-37. https://doi.org/10.1016/j.solener.03.108.
26. Bhattacharyya K, Mane G, Rane V et al. Selective CO_2 Photoreduction with Cu-Doped TiO2 Photocatalyst: Delineating the Crucial Role of Cu-Oxidation State and Oxygen Vacancies. J Phys Chem. 2021;125(3). https://doi.org/10.1021/acs.jpcc.0c08441
27. Kubiak A, Bielan Z, Bartkowiak A et al. Synthesis of Titanium Dioxide via Surfactant-Assisted Microwave Method for Photocatalytic and Dye-Sensitized Solar Cells Applications. Catalysts. 2020;10:586. https://doi.org/10.3390/catal10050586
28. Sudrajat H, Babel S, Ta A et al. Mn-doped TiO2 photocatalysts: Role, chemical identity, and local structure of dopant. J Phy Chem Sol. 2020;144:109517. https://doi.org/10.1016/j.jpcs.2020.109517
29. Bi X, Du G, Kalam A et al. Tuning oxygen vacancy content in TiO2 nanoparticles to enhance the photocatalytic performance. Chem Eng Sci. 2021;234:16440. https://doi.org/10.1016/j. ces.2021.116440
30. Pedroza-Herrera G, Medina-Ramírez I, Lozano-Alvarez J et al. Evaluation of the Photocatalytic Activity of Copper Doped TiO2 nanoparticles for the Purification and/or Disinfection of Industrial Effluents. Catal Tod. 2020;341:37-48. https://doi.org/10.1016/j.cattod.2018.09.017
31. Bartkowiak A, Korolevych O, Chiarello G et al. How Can the Introduction of Zr^{4+} Ions into TiO_2 Nanomaterial Impact the DSSC Photoconversion Efficiency? A Comprehensive Theoretical and Experimental Consideration. Mater. 2021;14(11):2955. https://doi.org/10.3390/ ma14112955
32. Bramhankar T, Pawar S, Shaikh J et al. Effect of Nickel-Zinc Co-doped TiO2 blocking layer on performance of DSSCs. J All Comp. 2020;817:152810. https://doi.org/10.1016/j.jallcom.2019.152810
33. Kumaravel V, Rhatigan S, Mathew S et al. Mo doped TiO_2: impact onoxygen vacancies, anatase phase stability and photocatalytic activity. J Phy Mater. 2020;3(2020):025008. https://doi.org/10.1088/2515-7639/ab749c

34. Mamakhel A, Yu J, Søndergaard-Pedersen F et al. Facile synthesis of brookite TiO_2 nanoparticles. Chem Comm. 2020;56(95):15084-87. https://doi.org/10.1039/D0CC06795D
35. Gnida P, Jarka P, Chulkin P et al. Impact of TiO_2 Nanostructures on Dye-Sensitized Solar Cells Performance. Mater. 2021;14(7):1633. https://doi.org/10.3390/ ma14071633.
36. Aleksandra B, Oleksandr K, Gian L et al. Experimental and theoretical insight into DSSCs mechanism influenced by different doping metal ions. Appl Surf Sci. 2022;597:153607. https://doi.org/10.1016/j.apsusc.2022.153607